Tunable and Reconfigurable Bandstop Microwave Photonic Filter Based on Integrated Microrings and Mach–Zehnder Interferometer

Dengke Zhang, Xue Feng, Xiangdong Li, Kaiyu Cui, Fang Liu, and Yidong Huang, *Member, IEEE*

***Abstract*—A bandstop microwave photonic filter is experimentally demonstrated with integrated optical processor fabricated on silicon-on-insulator substrate. The optical processor consists of microrings and a Mach–Zehnder interferometer so that two bandstop responses are produced for processing two sidebands separately. With such a structure, tunable and reconfigurable bandstop MPFs can be easily realized by thermally tuning the resonant wavelength of microrings. According to the experimental results, the operating frequency and 10-dB bandwidth can be tuned within the range of 7–34 GHz and 1.85–4.55 GHz, respectively.**

***Index Terms*—Integrated optics, microwave photonic filters, microring resonators, tunability, reconfigurability.**

I. Introduction

MICROWAVE photonic filters (MPFs) can perform the microwave (even millimeter wave) signal processing in the optical domain with photonic devices. So it could be widely applied on radar, satellite or wireless communications with some unique and attractive characters, including low loss, wide bandwidth, and immunity to electromagnetic interference, etc. [1]–[4]. In previous reports [5]–[8], the MPFs with fiber devices are dominative and the operation principle is based on beam splitting, time delay, and beam combining, which is similar to so-called transverse filter. For such MPFs, the operation frequency is determined by the time delay. Thus, rather long fiber coil is usually adopted to achieve long time delay from hundreds of picosecond to tens of nanosecond so that the operating frequency could be within the range of megahertz–gigahertz. Since the fiber coil suffers from ambient variation, most of such MPFs operate under incoherent condition to improve stability. As mentioned in [1], such incoherent MPFs also are restricted in the responses due to positive filter coefficients and the typical periodic responses may cause cross-talk from undesired signal within other transmission band [9].

Recently, owning to great progress on photonic integrated circuit [10], MPFs with integrated silicon optical processors were also proposed and demonstrated [11]–[19]. The most straightforward advantages are low cost, small footprint, and potential for integration with other devices, including modulators and photodetectors. For example, integrated delay lines were adopted instead of long fiber coils [11]–[13]. In [11], with a tunable photonic crystal waveguide, the operating frequency of bandpass/notch MPF could be tuned from 10 to 40 GHz while the length of delay line is only 1.5 mm. In [12], a notch MPF with tuned bandwidth of 0.03-1 GHz was demonstrated by employing compact microring with radius of only 250 μm. Both of the above two reports are still incoherent MPFs. Actually, it is also possible to implement coherent MPFs with integrated optoelectronic devices since the stability can be assured if all components could be integrated on a small chip. With coherent optical processor, more freedom could be utilized to achieve more flexible MPF response as the field summations in terms of both magnitude and phase shift.

For coherent integrable MPFs, a typical and pioneering work was completed by B. Pile and G. Taylor. They presented the operation principle of MPFs with microring and analyses of the noise and distortion performance [14]. After that, there were several experimental demonstrations of microring based MPFs with tunability or reconfigurability [15]–[19]. In [15], a bandpass MPF with single peak was demonstrated with tuning bandwidth of 5–15 GHz and operating frequency of 18–40 GHz. In [18], an MPF with a single notch is achieved with tuning bandwidth of 2–4 GHz and operating frequency of 3–18 GHz. These results indicate that compact microrings provide an attractive platform to improve performance and manipulation of an MPF. This is due to two important characteristics of microring resonator: first, self-response of microring is an assembled resonant response since beam splitting, time delay, and coherent beam combining could be accomplished within a single ring resonator. So microring can be directly transplanted to process microwave signal in optical domain independently; secondly, single resonant response and high operating frequency can be obtained due to short cavity length and small footprint. Thus there could be only one resonant peak within the microwave band and the crosstalk from other transmission band could be avoided. Particularly, flexible tuning could be readily achieved for MPFs implemented with silicon microrings since both thermo-optic or plasma-dispersion effect could be employed and easily realized [10].

Manuscript received July 9, 2013; revised September 25, 2013; accepted October 17, 2013. Date of publication October 23, 2013; date of current version November 6, 2013. This work was supported in part by the National Basic Research Program of China (No. 2011CBA00608, 2011CBA00303), in part by the National Natural Science Foundation of China (Grant Nos. 61036011 and 61036010), and in part by the Project of Science and Technology on Communication Information Security Control Laboratory. *(Corresponding author: X. Feng.)*

The authors are with Tsinghua National Laboratory for Information Science and Technology, Department of Electronic Engineering, Tsinghua University, Tsinghua University, Beijing 100084, China. (e-mail: zdk08@mails.tsinghua.edu.cn; x-feng@tsinghua.edu.cn; 2007lixiangdong@163.com; kaiyucui@tsinghua.edu.cn; liu_fang@tsinghua.edu.cn; yidonghuang@tsinghua.edu.cn).

Color versions of one or more of the figures in this paper are available online at http://ieeexplore.ieee.org.

Digital Object Identifier 10.1109/JLT.2013.2287091

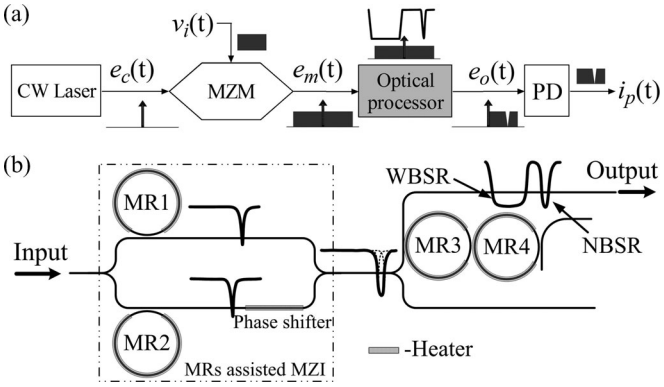

Fig. 1. (a) Schematic of a typical MPF and (b) the proposed optical processor to achieve a bandstop MPF.

According to the application requirements, these reported MPFs with microrings could be classed as bandpass and bandstop (or notch) filters. For both of them, the central operating frequency and bandwidth are in great need of tuning when the signals or noises may be random and unpredictable. However, it is difficult to simultaneously achieve tunability and reconfigurability within wide range. In our previous work, a tunable and reconfigurable bandpass MPF based on integrated optical processor is proposed and experimentally demonstrated on a silicon-on-insulator (SOI) substrate [15]. According to the experimental results, the operating frequency and 3-dB bandwidth can be tuned from 18 to 40 GHz and from 5 to 15 GHz, respectively. This is due to the novel integrated optical processor based on microrings (MRs) and Mach–Zehnder interferometer (MZI), which is utilized to produce two bandpass responses for processing optical carrier and sideband separately. For a bandpass MPF, the wanted signal can pass through the filter and be processed. For a bandstop/notch MPFs, only the interference signal or noise within a narrow bandwidth is filtered out. Obviously, the designing and operation principles would be quite different for such two types of MPFs.

In this study, a bandstop MPF with integrated microrings and Mach–Zehnder interferometer is proposed and demonstrated in succession. Due to the controlling flexibility, both tunability and reconfigurability can be achieved by tuning resonance wavelength of microrings. First, our designed optical structure and the operating principle of the proposed MPFs are introduced. Meanwhile, how to vary the operating frequency and bandwidth of MPF are explained in detail. Second, the tunability and reconfigurability of such MPF are demonstrated with a series of experiments. Then there are some discussions about improvements of the performance and limitations of such kind of MPFs. Finally, a summary is presented.

II. Proposed Structure and Operating Principle

Fig. 1(a) shows the typical scheme of an MPF. The microwave signal is modulated on optical carrier, processed by an optical processor and detected by a photodetector (PD). With intensity modulation, the optical spectrum after Mach–Zehnder modulator (MZM) includes two parts: carrier and two sidebands. In our previous work about the bandpass MPF [15], it was proved that carrier and sidebands can be processed separately by an optical processor based on MRs and MZI with two narrow bandpass responses, which takes the advantage of high quality factor (narrow bandwidth). In this study, the optical processor is also based on MRs and MZI. The difference is that two bandstop responses with different bandwidth are utilized. Thus, as shown in Fig. 1(a), if the carrier is set at a proper position between the two bandstop responses of the optical processor, one of sideband is suppressed by the bandstop response with wider bandwidth while the other sideband could be processed fully by the narrower bandstop response (denoted as operation channel). Then after photodetection, the processed signal in optical domain could be converted back to microwave signal. With such processing procedure in optical domain, a bandstop MPF is obtained.

The proposed optical processor is shown in Fig. 1(b), which consists of a MZI and four MRs (MR1–MR4). The whole processor can be divided into two units. The first one is enclosed by a rectangle on the left side of Fig. 1(b), which is denoted as two MRs assisted MZI (MRAMZI) and used to obtain narrow bandstop response (NBSR). The other one is a second-order series-coupled microrings (SCMRs) at the right side, which is used for generating wide bandstop response (WBSR). After such an optical processor, there would be two bandstop responses, which are denoted as WBSR and NBSR (marked in Fig. 1(b)). Here, the optical carrier should be properly settled between WBSR and NBSR so that unutilized sideband signal can be the suppressed by WBSR while the other sideband could be processed by NBSR. Thus, the operating frequency of MPF is determined by the frequency interval between the carrier and the center of the NBSR while the bandwidth is determined by the bandwidth of NBSR. Thus, tunability and reconfigurability of MPF can be achieved by tuning the frequency interval and bandwidth of NBSR independently.

To design the proper structural parameters and demonstrate the operation principles in detail, some numerical simulations are carried out. The proposed optical processor is considered as fabricated on SOI substrate, while the MZI and MRs are formed by shallow ridge silicon waveguides with width of 1 μm, total thickness of 220 nm, and ridge height of 60 nm. The radius of all four microrings is 100 μm, and Si refractive index of microrings is assumed to be tuned. Such parameters could ensure that fundamental mode with TE polarization is excited at wavelength around 1550 nm and the bending loss can be ignored while the propagation loss is considered as 3 dB/cm.

To obtain the microwave response of the MPFs, the optical response of optical processor should be deduced first. As shown in Fig. 1(b), the whole processor is divided into two connected units so that the assembled optical transfer function $(H_{\rm O}(\omega))$ can be obtained from amplitude transmissions of the MRAMZI $(T_{\rm MRAMZI})$ and second-order SCMRs $(T_{\rm SCMR})$ as:

$$H_{\rm O}(\omega) = T_{\rm MRAMZI} \cdot T_{\rm SCMR} \tag{1}$$

where the expressions of $T_{\rm MRAMZI}$ and $T_{\rm SCMR}$ can be found in the Appendix.

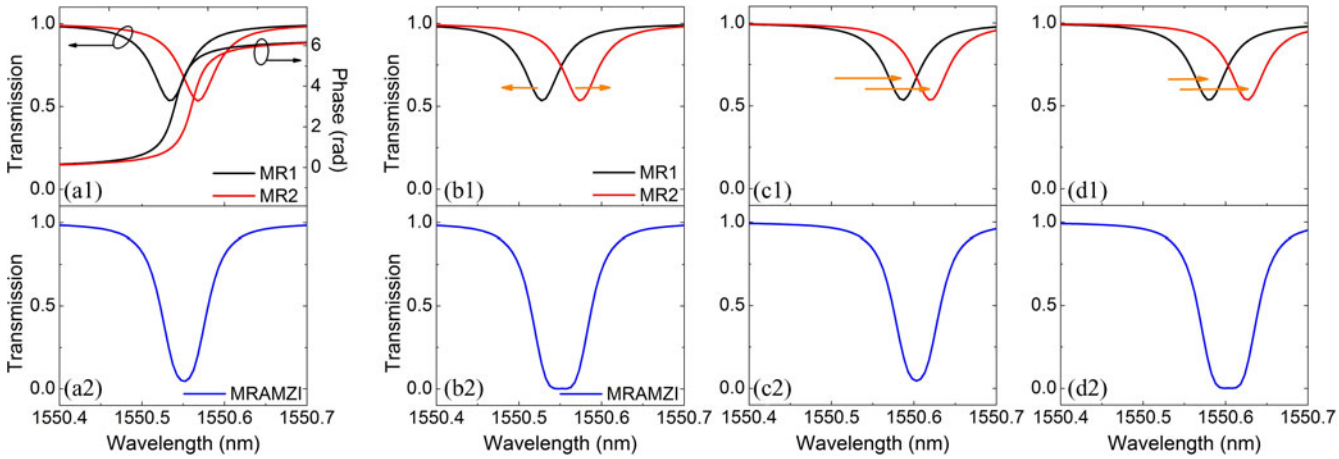

Fig. 2. (a1) Power transmissions and phase responses of MR1 and MR2, (a2) Optical power response of MRAMZI based on responses of MR1 and MR2 shown in (a1), (b1) Move the resonances of MR1 and MR2 oppositely with the same scale, (b2) Optical power response of MRAMZI corresponding to (b1), (c1) Move the resonances of MR1 and MR2 in the same direction with the same scale, (c2) Optical power response of MRAMZI corresponding to (c1), (d1) Move the resonances of MR1 and MR2 in the same direction but not the same value, and (d2) Optical power response of MRAMZI corresponding to (d1).

It has been mentioned that MRAMZI is used for processing useful sideband signal so that the tuning and reconfiguration are achieved by controlling this unit. For more clarity, the response of MRAMZI is analyzed in detail. With equation (A2) in the Appendix, T_{MRAMZI} is calculated and shown in Fig. 2(a2), which is obtained by adopting MR1 and MR2 with responses shown in Fig. 2(a1). It could be seen that there is a bandstop response with steep edge for the operation channel. From equation (A2) and Fig. 2(a1) and (a2), it can be found that the central wavelength (λ_{c}) and bandwidth (BW) of T_{MRAMZI} could be varied by tuning the resonant wavelength of MR1 and MR2 $(\lambda_{\mathrm{MR1}}$ and $\lambda_{\mathrm{MR2}})$. Specifically, λ_{c} and BW denote the median point and interval of λ_{MR1} and λ_{MR2}, respectively. Based on such relationships, the central wavelength and bandwidth of response of MRAMZI (corresponding to NBSR) can be tuned separately or simultaneously by adjusting resonance of MR1 and MR2. When only tuning the BW, λ_{MR1} and λ_{MR2} are varied with the same value but in the opposite direction. Fig. 2(b1) and 2(b2) show the results for only tuning BW while λ_{c} is nearly constant. Here, the BW is extended by decreasing λ_{MR1} and increasingλ_{MR2}. For tuning the λ_{c}, λ_{MR1} and λ_{MR2} are varied with the same value and the same direction. Fig. 2(c1) and 2(c2) show the case of only tuning λ_{c}. It could be found that the λ_{c} is increased by increasing λ_{MR1} and λ_{MR2} at the same time. Moreover, λ_{c} and BW can be tuned simultaneously by proper adjusting of λ_{MR1} and λ_{MR2}. Fig. 2(d1) and 2(d2) are an example that the BW is extended and the λ_{c} is increased.

With the T_{MRAMZI} for processed sideband and T_{SCMR} for suppressed sideband, the assembled transfer function could be calculated. By proper setting the resonant wavelength of MR1–MR4, two bandstop responses could be achieved and an example is demonstrated in Fig. 3. Fig. 3(a) and (b) are the optical responses of MRAMZI and second-order SCMRs, respectively, and optical response shown in Fig. 3(c) is the assembled response. It could be found that there are two bandstop responses in one free spectral region (FSR) marked in the dashed box.

With the optical response, the microwave response of MPF based on the proposed optical processor could be deduced.

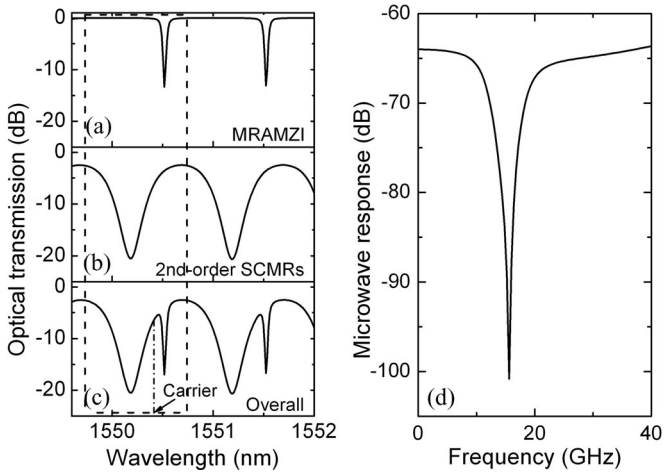

Fig. 3. (a) Optical transmission of MRAMZI, (b) Optical transmission of second-order SCMRs, (c) Optical transmission of the whole optical processor, (d) Microwave response of MPF based on optical processor with response shown in (c). The dashed box in (a)–(c) shows the region of an FSR.

According to [14], a microwave transfer function $H_{\mathrm{M}}(\omega_{\mathrm{m}})$ with double-sideband plus carrier (DSB + C) modulation is given by:

$$H_{\mathrm{M}}(\omega_{\mathrm{m}}) \approx \frac{\Re P_{\mathrm{c}} R_{\mathrm{L}}}{v_{\mathrm{m}}} J_0\left(\frac{\pi v_{\mathrm{m}}}{V_\pi}\right) J_1\left(\frac{\pi v_{\mathrm{m}}}{V_\pi}\right) \times \left(H_{\mathrm{O}}(\omega_{\mathrm{c}}) H_{\mathrm{O}}^*(\omega_{\mathrm{c}} - \omega_{\mathrm{m}}) + H_{\mathrm{O}}^*(\omega_{\mathrm{c}}) H_{\mathrm{O}}(\omega_{\mathrm{c}} + \omega_{\mathrm{m}})\right) \quad (2)$$

where ω_{c} and ω_{m} are optical carrier and microwave signal frequency, respectively, $\Re$ is the responsivity of an ideal photodetector, P_{c} is the input laser power, R_{L} is the load resistance, v_{m} is the amplitude of microwave signal, V_π is the half-wave voltage of modulator, $J_{\mathrm{n}}(\cdot)$ is the nth-order Bessel function of the first kind, and $H_{\mathrm{O}}(\omega)$ is the optical response of optical processor, which could be calculated by equation (1). Fig. 3(d) shows the calculated microwave response with the optical response shown in Fig. 3(c). Here, the adopted carrier wavelength is marked in Fig. 3(c) and the other simulation parameters of MPF are set as $\Re = 0.5$ A/W, $P_{\mathrm{c}} = 10$ mW, $R_{\mathrm{L}} = 50\,\Omega$, $V_\pi = 5$ V, and

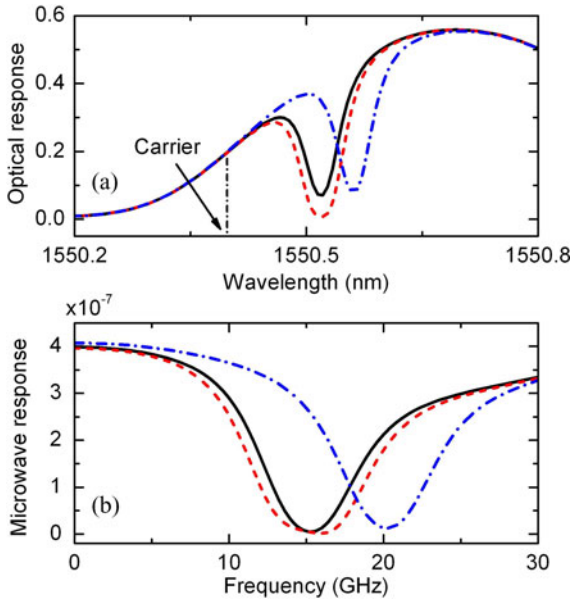

Fig. 4. (a) Tuning MRAMZI from the assembled initial optical response (in black line) to wider bandwidth [in red line, according to MR responses in Fig. 2(b1) and (b2)] or longer resonance wavelength (in blue line, according to MR responses in Fig. 2(c1) and (c2)), (b) and the corresponding response of MPF is tuned from the initial response (in black line) to response with wider bandwidth (in red line) or higher operating frequency (in blue line).

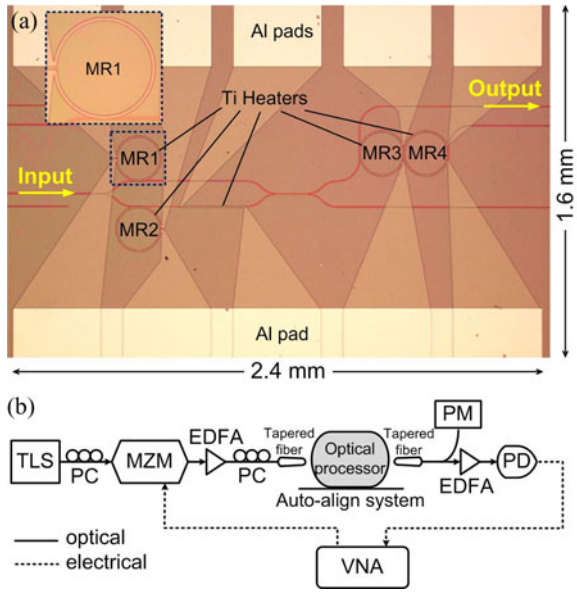

Fig. 5. (a) Optical micrograph of the proposed optical processor and the inset is an enlarged image of MR1. (b) Schematic of the measurement system.

$v_{\mathrm{m}} = (0.5/\pi)$ V. Due to the double- sideband modulation and residual band of WBSR, the shape of MPF response is a little different to that of NBSR, especially in the slope of flat range of responses, which could be found in Fig. 3(c) and (d).

As shown in Fig. 2(a1)–(d2), the bandwidth and central operating wavelength of MRAMZI filter can be tuned independently or simultaneously. For the MPFs, the operating frequency is determined by the frequency interval between the central frequency of optical carrier and that of MRAMZI filter, while the bandwidth is determined directly by the response shape of MRAMZI filter. Thus, if the optical carrier is kept constant, the operating frequency can be tuned by adjusting the central wavelength of MRAMZI filter (tunability) and the bandwidth can be varied by adjusting the bandwidth of MRAMZI filter (reconfigurability). Here, simulation results for two typical cases are shown in Fig. 4 .When the optical response [see Fig. 4(a)] is tuned from black-curve to red-curve with wider bandwidth or blue-curve response with larger resonant wavelength, the corresponding response of MPF [see Fig. 4(b)] is tuned to wider bandwidth of 9 GHz (shown by the red-curve) or higher operating frequency of 20 GHz (shown by the blue-curve) while the initial bandwidth is 7 GHz and central frequency is 15 GHz (shown by the black-curve), respectively. These results indicate that both the central frequency and filter shape could be varied with our proposed optical processor.

III. Fabrication and Experimental Results

The proposed optical processor was fabricated on an SOI wafer (220-nm top silicon layer and 3-μm buried oxide layer) with electron-beam lithography, inductively coupled plasma etching, and depositing a 600-nm-thick SiO_2 cladding layer by plasma-enhanced chemical-vapor deposition. The heaters for tuning Si refractive index and pads for probe were sequentially patterned with photo-lithography, evaporation, and lift-off processes. The heaters are composed by 100-nm-thick Ti and electrical contact pads are composed by 100-nm-thick Ti and 200-nm-thick Al. The structural parameters of the shallow ridge waveguide are the same as those used in numerical simulations. The gap widths between the MR1(2) and arms of MZI are 400 nm while that are 25/50/25 nm for the second-order SCMRs. Only part of the microrings and one arm of the MZI are covered by heaters for thermal tuning. An optical micrograph of fabricated sample is shown in Fig. 5(a) and an enlarged image of MR1 is shown in the inset.

Fig. 5(b) is a schematic of the employed measurement system, which consists of a tunable laser source (TLS, 1350–1620 nm), two polarization controllers (PCs), a 40-Gbps $LiNbO_3$ Mach–Zehnder modulator (MZM, Codeon, Mach-40TM-005), two erbium-doped fiber amplifiers (EDFAs), and a high-precision auto-align optical testing system (SURUGA SEIKI, C7214-9015) with two tapered fibers. At the output ends, a power meter (PM, Agilent, 81624A) and a 50-GHz photodetector (PD, U2T, XPDV2120R) with a 40-GHz vector network analyzer (VNA, Agilent, E8363B) were used to measure the spectra.

By carefully tuning the heaters, proper resonances of microrings and required response of optical processor can be achieved. Fig. 6(a) is a measured optical spectrum with two bandstop responses in one FSR of about 120 GHz (shown in the dashed box). They are corresponding to the WBSR and NBSR in Fig. 1(b) and generated by the second-order SCMRs and MRAMZI, respectively. For microwave measurement, the optical carrier is settled at 1550.47 nm between WBSR and NBSR, and Fig. 6(b) is the measured microwave response. It could be seen that the bandstop MPF is operated at central frequency of 16.3 GHz and 10-dB bandwidth of 2.4 GHz.

TABLE I
COMPARISON OF THE FIGURES OF MERIT FOR SOME OTHER MPF IMPLEMENTATIONS

Type	Technology	10-dB Bandwidth(BW) /GHz	Operating frequency(OF) /GHz	OF tuning range / FSR /%
Coherent integrable MPFs	This work	1.85–4.55	7–34 (7–60 in theory)	21 (44 in theory)
	SOI-optical filter with microrings [18]	2–4	3–18	9
	SOI-optical filter with microrings and MZI [19]	0.3–0.4	2–15	30
Incoherent integrable MPFs	SOI-delay line with photonic crystal [11]	5	10–40	100
	SOI-delay line with microring [12]	0.03–1	19.92–20.02	77
	SOI-delay line with microring [13]	0.03	1.73–1.78	55
Incoherent common MPFs	Fiber-semiconductor optical amplifier [20]	0.002	30.005–30.014	100
	Fiber-simulated Brillouin scattering[21]	1	2.3–7.0	100
	Fiber-chirped Bragg grating[22]	0.5–1	1.1–2.1	47

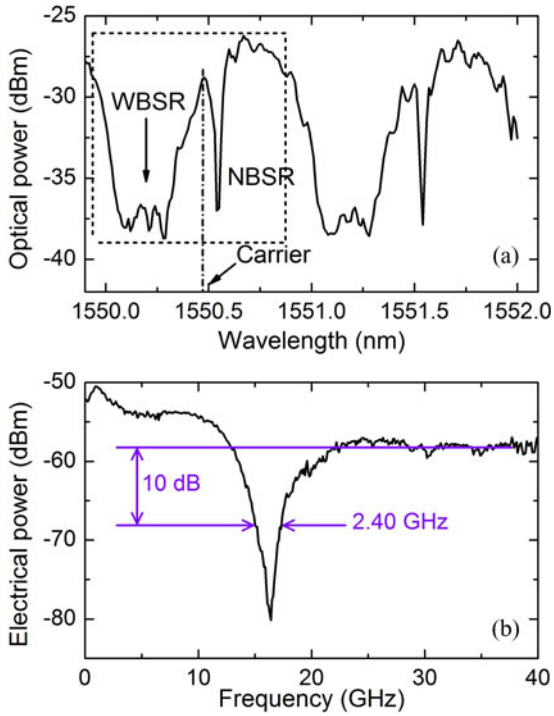

Fig. 6. (a) Measured optical response of the proposed optical processor and dashed box shows the region of a FSR. (b) Corresponding measured microwave response of MPF based on proposed optical processor.

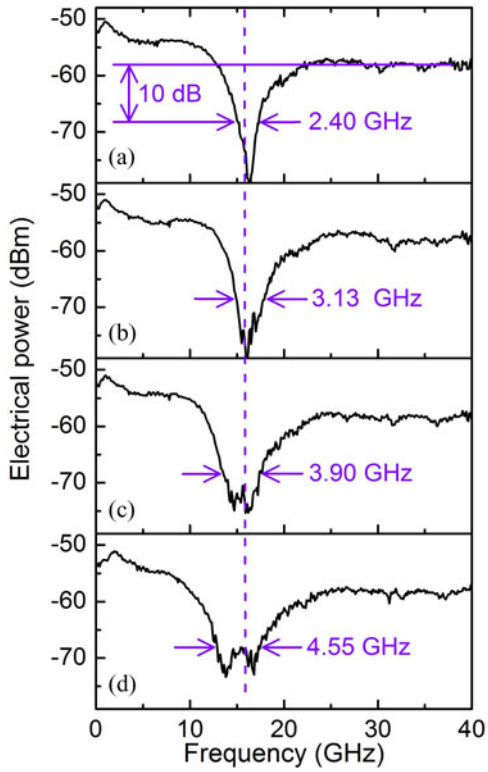

Fig. 7. The operating bandwidth is varied from 2.40 to 4.55 GHz with constant operating frequency of ~16 GHz.

As mentioned above, the operating bandwidth can be varied by changing the refractive index of MR1 and MR2 with heaters. In the measurement, opposite variation of thermal tuning power (proportional to the square of the voltage) are applied on MR1 and MR2 with the same value so that equal resonance shift of MR1 and MR2 is introduced in opposite directions. Then the bandwidth could be varied with constant operating frequency. As shown in Fig. 7(a–d), with the constant operating frequency of about 16 GHz, the 10-dB bandwidth could be varied from 2.40 to 4.55 GHz.

For tuning operating frequency of MPF, equal variation of thermal tuning power is applied on both MR1 and MR2. As a result nearly equal resonance shift (both value and direction) is introduced on both MR1 and MR2. Then operating frequency

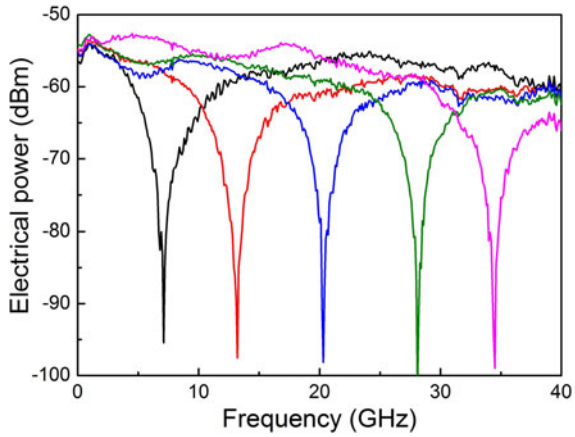

Fig. 8. Operating frequency is tuned from 7 to 34 GHz with the 10-dB bandwidth of ~2.2 GHz.

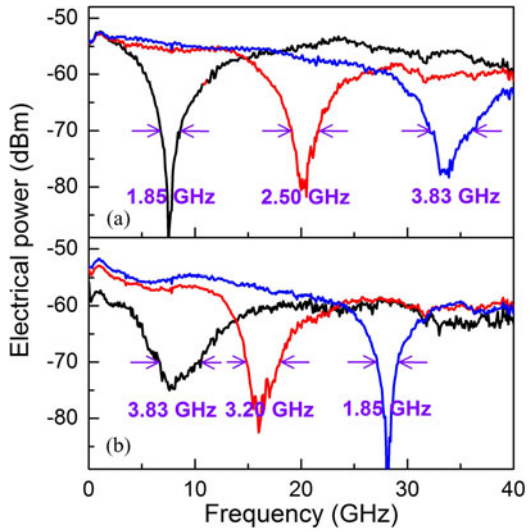

Fig. 9. (a) Operating frequency of MPFs is tuned to higher frequency with increased bandwidth. (b) Operating frequency of MPFs is tuned to higher frequency with decreased bandwidth.

of MPF is tuned while the MPF bandwidth keeps constant. As shown in Fig. 8, the operating frequency is tuned from 7 to 34 GHz while the 10-dB bandwidth is nearly constant at frequency of about 2.2 GHz.

Actually, the resonance of MR1 and MR2 could be tuned independently so that multiple combinations of operating frequency and bandwidth could be achieved by proper setting the thermal power applied on MR1 and MR2. In Fig. 9(a), the operating frequency is tuned to from 7.5 to 33.5 GHz and the 10-bandwidth is increased from 1.85 to 3.83 GHz. As a comparison, a reverse case is presented in Fig. 9(b), in which the 10-bandwidth is decreased from 3.83 to 1.85 GHz within the operating frequency range from 7.5 to 27.8 GHz.

IV. Discussion

In some previous works, tunable and reconfigurable bandstop/notch MPFs have been reported with cascaded microrings, integrated optical delay line, and fiber based devices. Table I shows the comparison between this study and them in terms of 10-dB bandwidth, operating frequency, and ratio between operating frequency tuning range and FSR. It could be found that our demonstrated MPF presents flexible tunability and reconfigurability within rather wide frequency range, especially comparing to incoherent integrable MPF and incoherent common MPF. It is due to the design of two bandstop responses and the fact that the response of microring is more sensitive to the thermal tuning than that of a waveguide or grating. While the ratio between operating frequency tuning range and FSR is still behind some of reported data of incoherent integrable MPF and incoherent common MPF, however, if single sideband modulation is adopted, this figure can be doubled in theory. In short, the proposed MPF has great potential in tunability and reconfigurability.

Still due to the resonant nature, microring is also very sensitive to ambient temperature variation. So the thermal stability for all microring devices is a crucial issue that must be considered. Till now, several approaches have been proposed to improve the thermal stability of microring, such as using feedback control [23] or special waveguide structure which is insensitive to temperature [24]. Thus, following with the development of these advanced technologies or novel methods, we believe that the stability could be solved in the near feature.

Since the filter shape of our proposed MPF is assembled by the response of MR1 and MR2, the bandwidth of MPF is determined by optical response of microrings. It is well known that the response of single microring is Lorentz's lineshape and then the band-edge of assembled response of NBSR is also Lorentz's lineshape-like. Thus the minimum bandwidth of our proposed MPF is ultimately limited by the Q-factor of microrings, which is determined by the coupling dissipation and intrinsic loss of microrings. If narrower bandwidth is needed, high accuracy fabrication process is required to reduce the scattering loss due to roughness of waveguide sidewall. Meanwhile, there is also a maximum value for achievable bandwidth. When the interval between the two resonances of MR1 and MR2 is increased, the interference would be weakened and the bandstop response of NBSR cannot be maintained so that the filter response of MPF may be split, which could be observed in Fig. 7(d). Specifically, there is a little split peak in the spectrum as the bandwidth is increased to 4.55 GHz. Thus this value is considered as the maximum bandwidth in our experiment. Otherwise, the filter shape would be deteriorated much more. If higher bandwidth is needed, the coupling coefficients between MR1(2) and arms of MZI should be increased.

For the operating frequency, there are also the minimum and maximum values. As aforementioned, the operating frequency is determined by the frequency interval between the central frequency of optical carrier and that of MRAMZI filter. Thus the minimum operating frequency is determined by the interval between WBSR and NBSR. In principle, the minimum value could approach zero if the band-edges of both WBSR and NBSR are sharp enough. However, the actual band-edges of our demonstrated MPF are Lorentz's lineshape-like so that the operating frequency cannot work well at the frequency range of 0.1 to 7 GHz. This can be improved by enhancing Q-factor of microrings with methods of increasing ring number of SCMR and decreasing ring coupling coefficients in MRAMZI [25]. On the other hand, the maximum operating frequency is limited by the FSR of optical processor. If the two signal sidebands of modulated light are within a FSR response ($2\omega_{\mathrm{m}} \leq \mathrm{FSR}$), the signal processing would not be affected by adjacent FSR responses so that the maximum operating frequency could be evaluated as half of the FSR ($\omega_{\mathrm{m}} \leq \mathrm{FSR}/2$). Generally, due to the short circumference of microrings, the FSR of the overall optical response is rather large (typically, for a silicon microring with radius of 10 μm, the FSR is about 1.3 THz around wavelength of 1550 nm). In this study, the FSR is about 120 GHz (according to the microring radius of 100 μm) so that the maximum operating frequency is about 60 GHz. However, in the experiment, the highest operating frequency is only about 40 GHz, which is

limited by bandwidth of VNA. As a reasonable perspective, we believe that if smaller radius of microrings is adopted, the proposed MPFs possess the potential in application of high frequency signal processing such as millimeter-wave signal of spectra of V-band (50–75 GHz) and W-band (75–110 GHz) [26]–[28].

From aspect of application, the insertion loss is also a critical parameter. The insertion loss of the integrated optical processor in our demonstrated MPF can be divided into three parts. The first one is from transmission loss at carrier wavelength due to not very sharp band-edge [sited at the band-edge of WSBR as shown in Fig. 3(c)], which can be improved by increasing ring number of SCMR and decreasing intrinsic loss of microrings. The second is from the Y-branch between WBSR and NBSR, which is used to monitor the signal after the NBSR in our fabricated sample. Actually, such Y-branch is not necessary for a practical device so that 3 dB insertion loss can be removed. The last part is the coupling loss between tapered fibers and chip. In our experiment, the averaged coupling loss is about 7 dB/facet. If optimization taper structures of Si waveguide are adopted, such loss can be greatly reduced and the typical value of coupling loss is only about 2 dB/facet [29]–[31]. Moreover, if the proposed optical processor is integrated with modulators and photodetectors, this part of insertion loss can also be removed.

V. Conclusion

In this study, a bandstop MPF with integrated optical processor is proposed and demonstrated experimentally. According to the experimental results, the operating frequency and 10-dB bandwidth of MPF can be tuned from 7 to 34 GHz and from 1.85 to 4.55 GHz, respectively. Since the modulator and detector could be integrated with our proposed optical processor on one SOI chip in principle, we believe that such kind of MPFs paves the way to all-optical integration on compact tunable and reconfigurable MPF.

Appendix

For MRAMZI, there are two through-output MRs (MR1 and MR2) with little difference on resonant wavelengths and overcoupled to each arm of MZI. To obtain optical response of MRAMZI, the microring resonator is analyzed by Fabry–Perot resonator model and the amplitude transmission $T_{\mathrm{MR1(2)}}$ of through-output of the MR1 (2) can be deduced as

$$T_{\mathrm{MR1(2)}} = \frac{t_{\mathrm{MR1(2)}} - a \cdot e^{-j(\omega n_{\mathrm{eff}} L/c)}}{1 - t_{\mathrm{MR1(2)}} a \cdot e^{-j(\omega n_{\mathrm{eff}} L/c)}} \tag{A1}$$

where ω is optical frequency, c is the light speed in vacuum, L is microring circumference, a is the single-pass amplitude transmission, n_{eff} is the effective refractive index of ring waveguide, and $t_{\mathrm{MR1(2)}}$ presents self-coupling amplitude coefficient between the arm and MR1(2). Fig. 2(a1) shows the typical intensity and phase responses of MR1 and MR2, the solid and dashed line correspond to MR1 and MR2, respectively. Then, the optical transfer function of MRAMZI can be written as

$$T_{\mathrm{MRAMZI}} = (T_{\mathrm{MR1}} + T_{\mathrm{MR2}})/2. \tag{A2}$$

The bandstop response of SCMR can be deduced by the followed expressions:

$$T_{\mathrm{SCMR}} = T_{\mathrm{MR3}} + \frac{D_{\mathrm{MR3}} D'_{\mathrm{MR3}} t_{\text{d-MR4}} a \cdot e^{-j(\omega n_{\mathrm{eff}} L/c)}}{1 - T'_{\mathrm{MR3}} t_{\text{d-MR4}} a \cdot e^{-j(\omega n_{\mathrm{eff}} L/c)}} \tag{A3a}$$

$$T_{\mathrm{MR3(4)}} = \frac{t_{\text{i-MR3(4)}} - t_{\text{d-MR3(4)}} a \cdot e^{-j(\omega n_{\mathrm{eff}} L/c)}}{1 - t_{\text{i-MR3(4)}} t_{\text{d-MR3(4)}} a \cdot e^{-j(\omega n_{\mathrm{eff}} L/c)}} \tag{A3b}$$

$$D_{\mathrm{MR3(4)}} = -\frac{\kappa_{\text{i-MR3(4)}} \kappa_{\text{d-MR3(4)}} \sqrt{a} \cdot e^{-j(\omega n_{\mathrm{eff}} L/c)/2}}{1 - t_{\text{i-MR3(4)}} t_{\text{d-MR3(4)}} a \cdot e^{-j(\omega n_{\mathrm{eff}} L/c)}} \tag{A3c}$$

where $t_{\mathrm{i(d)\text{-}MR3(4)}}$ and $\kappa_{\mathrm{i(d)\text{-}MR3(4)}}$ present self- and cross-coupling amplitude coefficients between the input (drop) waveguide and the waveguide of MR3(4), respectively, and they should satisfy $t^2_{\mathrm{i(d)\text{-}MR3(4)}} + \kappa^2_{\mathrm{i(d)\text{-}MR3(4)}} = 1$, and D'_{MR3} and T'_{MR3} represent the inverse response of MR3 when light is injected from drop-port, which can be deduced referring to equations (A3b) and (A3c).

Acknowledgment

The authors would like to thank Dr. W. Zhang, Dr. Q. Zhou, and Z. F. Liu for their valuable discussions and helpful comments.

References

[1] J. Capmany, B. Ortega, and D. Pastor, "A tutorial on microwave photonic filters," *J. Ligthw. Technol.*, vol. 24, pp. 201–229, Jan. 2006.
[2] T. Berceli and P. R. Herczfeld, "Microwave photonics-a historical perspective," *IEEE Trans. Microw. Theory Tech.*, vol. 58, no. 11, pp. 2992–3000, Nov. 2010.
[3] R. A. Minasian, "Photonic signal processing of microwave signals," *IEEE Trans. Microw. Theory Tech.*, vol. 54, no. 2, pp. 832–846, Feb. 2006.
[4] A. J. Seeds and K. J. Williams, "Microw. photon," *J. Ligthw. Technol.*, vol. 24, pp. 4628–4641, Dec. 2006.
[5] D. Pastor, B. Ortega, J. Capmany, P. Y. Fonjallaz, and M. Popov, "Tunable microwave photonic filter for noise and interference suppression in UMTS base stations," *Electron. Lett.*, vol. 40, pp. 997–999, Aug. 2004.
[6] D. B. Hunter, R. A. Minasian, and P. A. Krug, "Tunable optical transversal filter based on chirped gratings," *Electron. Lett.*, vol. 31, pp. 2205–2207, Dec. 1995.
[7] D. B. Hunter and R. A. Minasian, "Tunable microwave fiber-optic bandpass filters," *IEEE Photon. Technol. Lett.*, vol. 11, no. 7, pp. 874–876, Jul. 1999.
[8] J. Capmany, D. Pastor, and B. Ortega, "New and flexible fiber-optic delay-line filters using chirped Bragg gratings and laser arrays," *IEEE Trans. Microw. Theory Tech.*, vol. 47, no. 7, pp. 1321–1326, Jul. 1999.
[9] J. Capmany, "Microwave photonic filters," in *Proc. Opt. Fiber Commun. Conf.*, Mar. 2012, pp. 1–47, Paper. OW3I.4.
[10] A. Barkai, Y. Chetrit, O. Cohen, R. Cohen, N. Elek, E. Ginsburg, S. Litski, A. Michaeli, O. Raday, and D. Rubin, "Integrated silicon photonics for optical networks [Invited]," *J. Opt. Netw.*, vol. 6, pp. 25–47, Jan. 2007.
[11] J. Sancho, J. Bourderionnet, J. Lloret, S. Combrié, I. Gasulla, S. Xavier, S. Sales, P. Colman, G. Lehoucq, and D. Dolfi, "Integrable microwave filter based on a photonic crystal delay line," *Nat. Commun.*, vol. 3, p. 1075, Sep. 2012.
[12] J. Lloret, J. Sancho, M. Pu, I. Gasulla, K. Yvind, S. Sales, and J. Capmany, "Tunable complex-valued multi-tap microwave photonic filter based on single silicon-oninsulator microring resonator," *Opt. Exp.*, vol. 19, pp. 12402–12407, Jun. 2011.
[13] M. Burla, D. Marpaung, L. M. Zhuang, C. Roeloffzen, M. R. Khan, A. Leinse, M. Hoekman, and R. Heiderman, "On-chip CMOS compatible

reconfigurable optical delay line with separate carrier tuning for microwave photonic signal processing," *Opt. Exp.*, vol. 19, pp. 21475–21484, Oct. 2011.

[14] B. Pile and G. Taylor, "An investigation of the operation and performance of coherent microwave photonic filters," *IEEE Trans. Microw. Theory Tech.*, vol. 57, no. 2, pp. 487–495, Feb. 2009.

[15] D. Zhang, X. Feng, and Y. Huang, "Tunable and reconfigurable bandpass microwave photonic filters utilizing integrated optical processor on silicon-on-insulator substrate," *IEEE Photon. Technol. Lett.*, vol. 24, no. 17, pp. 1502–1505, Sep. 2012.

[16] J. Palaci, G. E. Villanueva, J. V. Galan, J. Marti, and B. Vidal, "Single bandpass photonic microwave filter based on a notch ring resonator," *IEEE Photon. Technol. Lett.*, vol. 22, no. 17, pp. 1276–1278, Sep. 2010.

[17] D. Zhang, X. Feng, and Y. Huang, "Reconfigurable microwave photonic filter based on parallel-cascaded microrings assisted with a Mach-Zehnder interferometer," *J. opt.*, vol. 14, 065502, pp. 1–5, May 2012.

[18] J. Dong, L. Liu, D. Gao, Y. Yu, A. Zheng, T. Yang, and X. Zhang, "Compact notch microwave photonic filters using on-chip integrated microring resonators," *IEEE Photon. J.*, vol. 5, no. 2, 5500307, pp. 1–7, Apr. 2013.

[19] M. S. Rasras, K. Y. Tu, D. M. Gill, Y. K. Chen, A. E. White, S. S. Patel, A. Pomerene, D. Carothers, J. Beattie, M. Beals, J. Michel, and L. C. Kimerling, "Demonstration of a tunable microwavep Photonic notch filter using low-loss silicon ring resonators," *J. Ligthw. Technol.*, vol. 27, pp. 2105–2110, Jun. 2009.

[20] W. Xue, S. Sales, J. Mork, and J. Capmany, "Widely tunable microwave photonic notch filter based on slow and fast light effects," *IEEE Photon. Technol. Lett.*, vol. 21, no. 3, pp. 167–169, Feb. 2009.

[21] A. Loayssa, J. Capmany, M. Sagues, and J. Mora, "Demonstration of incoherent microwave photonic filters with all-optical complex coefficients," *IEEE Photon. Technol. Lett.*, vol. 18, no. 16, pp. 1744–1746, Aug. 2006.

[22] J. Wang and J. Yao, "A tunable photonic microwave notch filter based on all-optical mixing," *IEEE Photon. Technol. Lett.*, vol. 18, no. 2, pp. 382–384, Jan. 2006.

[23] K. Padmaraju, J. Chan, L. Chen, M. Lipson, and K. Bergman, "Thermal stabilization of a microring modulator using feedback control," *Opt. Exp.*, vol. 20, pp. 27999–28008, Dec. 2012.

[24] S. S. Djordjevic, K. Shang, B. Guan, S. T. Cheung, L. Liao, J. Basak *et al.*, "CMOS-compatible, athermal silicon ring modulators clad with titanium dioxide," *Opt. Exp.*, vol. 21, pp. 13958–13968, Jun. 2013.

[25] W. D. Sacher and J. K. S. Poon, "Characteristics of microring resonators with waveguide-resonator coupling modulation," *J. Ligthw. Technol.*, vol. 27, pp. 3800–3811, Sep. 2009.

[26] A. Stohr, A. Akrout, R. Bu , B. Charbonnier, F. van Dijk, A. Enard, S. Fedderwitz, D. J ger, M. Huchard, and F. Lecoche, "60 GHz radio-over-fiber technologies for broadband wireless services [Invited]," *J. Opt. Netw.*, vol. 8, pp. 471–487, May. 2009.

[27] H. S. Chung, S. H. Chang, J. D. Park, M. J. Chu, and K. Kim, "Transmission of multiple HD-TV signals over a wired/wireless line millimeter-wave link with 60 GHz," *J. Ligthw. Technol.*, vol. 25, pp. 3413–3418, Nov. 2007.

[28] A. Jebril, M. Lucente, E. Re, T. Rossi, M. Ruggieri, C. Sacchi, and V. Dainelli, "Perspectives of W-Band for space communications," in *Proc. IEEE Aerosp. Conf.*, Mar. 2007, pp. 1301–1312.

[29] J. N. Caspers, A. W. MacKay, and J. K. Poon, "Short efficient non-adiabatic spot-size converters by mode interference in silicon-on-insulator waveguides," in *Proc. Opt. Fiber Commun. Conf.*, Mar. 2012, pp. 1–3, Paper OTu2I.6.

[30] M. Wood, P. Sun, and R. M. Reano, "Compact cantilever couplers for low-loss fiber coupling to silicon photonic integrated circuits," *Opt. Exp.*, vol. 20, pp. 164–172, Jan. 2012.

[31] Q. Fang, J. F. Song, T.-Y. Liow, L. Jia, X. Luo, M. B. Yu, and G. Q. Lo, "Cleaved fiber-to-nano waveguide mode converter for silicon photonics devices," in *Proc. Photon. Global Conf.*, Dec. 2012, Paper 1.3E.5.

Authors' biographies not available at the time of publication.